High-mobility two-dimensional electron gases at oxide interfaces: Origin and opportunities

2013 Chinese Phys. B 22 116803

(http://iopscience.iop.org/1674-1056/22/11/116803)

TOPICAL REVIEW — Magnetism, magnetic materials, and interdisciplinary research

High-mobility two-dimensional electron gases at oxide interfaces: Origin and opportunities

Chen Yun-Zhong(陈允忠)[a)†], Nini Pryds[a)], Sun Ji-Rong(孙继荣)[b)], Shen Bao-Gen(沈保根)[b)], and Søren Linderoth[a)]

[a)] *Department of Energy Conversion and Storage, Technical University of Denmark, Risø Campus, Roskilde* 4000, *Denmark*
[b)] *Beijing National Laboratory for Condensed Matter Physics, State Key Laboratory for Magnetism, Institute of Physics, Chinese Academy of Sciences, Beijing* 100190, *China*

(Received 2 September 2013)

Our recent experimental work on metallic and insulating interfaces controlled by interfacial redox reactions in $SrTiO_3$-based heterostructures is reviewed along with a more general background of two-dimensional electron gas (2DEG) at oxide interfaces. Due to the presence of oxygen vacancies at the $SrTiO_3$ surface, metallic conduction can be created at room temperature in perovskite-type interfaces when the overlayer oxide ABO_3 has Al, Ti, Zr, or Hf elements at the *B* sites. Furthermore, relying on interface-stabilized oxygen vacancies, we have created a new type of 2DEG at the heterointerface between $SrTiO_3$ and a spinel γ-Al_2O_3 epitaxial film with compatible oxygen ion sublattices. This 2DEG exhibits an electron mobility exceeding 100000 $cm^2 \cdot V^{-1} \cdot s^{-1}$, more than one order of magnitude higher than those of hitherto investigated perovskite-type interfaces. Our findings pave the way for the design of high-mobility all-oxide electronic devices and open a route toward the studies of mesoscopic physics with complex oxides.

Keywords: oxide interfaces, two-dimensional electron gas (2DEG), $SrTiO_3$, oxygen vacancies

PACS: 68.47.Gh, 73.20.–r, 81.15.Fg **DOI:** 10.1088/1674-1056/22/11/116803

1. Introduction

The realization of high-mobility two-dimensional electron gases (2DEGs) in epitaxially grown heterostructures made of traditional semiconductors is at the heart of present electronics, and it has led to a wealth of new physical discoveries as well as new electronic and photonic devices over the past few decades, from p–n junctions to field-effect transistors and more recently to quantum devices, just to name a few. Currently, widespread interest has arisen in designing heterostructures with complex oxides instead of the traditional semiconductors. Unlike electrons in semiconductors, those in complex oxides with partially occupied d orbitals interact strongly with one another and with the lattice. This gives rise to a variety of extraordinary electronic properties, such as high-temperature superconductivity, colossal magnetoresistance, ferromagnetism, ferroelectricity, and multiferroicity. Therefore, the discovery of 2DEGs at well-defined interfaces between insulating complex oxides provides an opportunity for a new generation of all-oxide electronics. Particularly, the 2DEG at the interface between two perovskite insulators, represented by the formula ABO_3, has attracted significant attention. The high-mobility 2DEGs at atomically engineered complex oxide interfaces are expected to provide a wealth of opportunities to study mesoscopic physics with strongly correlated electrons confined in nanostructures, and they also show promise for all-oxide devices with functionalities much richer than those found in the conventional semiconductor devices.[1,2]

Much as silicon is the basis of the conventional electronics, strontium titanate ($SrTiO_3$, STO), a wide band gap insulator (band gap 3.2 eV), has been suggested as the foundation of the emerging field of oxide electronics. Particularly, the accessibility of regular single-TiO_2-terminated STO substrates[3,4] has triggered the possibility to fabricate complex oxide heterostructures with atomic-scale-flat interfaces through controlled film growth techniques, such as pulsed laser deposition (PLD)[5,6] and molecular beam epitaxy (MBE),[7,8] where the film growth process can be *in-situ* monitored by reflection high energy electron diffraction (RHEED). In 2004, by the epitaxial growth of another band gap insulator $LaAlO_3$ (LAO, band gap 5.6 eV) on TiO_2-terminated STO substrate, a metallic state was found at the interface between the two insulators (LAO/STO).[9] Since then, many other perovskite-type heterostructures are found to hold similar interfacial 2DEGs as long as STO is involved as the substrate, for instance, $LaTiO_3$/STO,[10] $GdTiO_3$/STO,[11] $LaGaO_3$/STO,[12] and so on. Moreover, a series of intriguing physical properties, such as, two-dimensional superconductivity,[13] magnetism,[14] and field-induced insulator-metal transition,[15–17] have also been observed at these oxide interfaces.

Due to the fascinating physics and potential device applications, extensive research activities, both experimental

†Corresponding author. E-mail: yunc@dtu.dk

and theoretical,[18–22] have been focused on the 2DEG at perovskite-type oxide interfaces, especially for the LAO/STO system. However, many important issues remain open. One primary question is: what are the origin and the underlying mechanism of the 2DEG at the LAO/STO oxide interface? The conduction of the LAO/STO heterostructure has been found to depend strongly on the growth parameters, particularly the partial pressure of oxygen, P_{O_2}, during the film growth. At P_{O_2} of 1×10^{-4} Pa and a typical deposition temperature of 800 °C, a quite high carrier density on the order of 4×10^{16} cm^{-2}, as well as a relative high mobility on the order of $(1–2)\times10^{4}$ cm$^2\cdot$V$^{-1}\cdot$s^{-1} at 2 K, is routinely obtained.[9,23,24] However, samples subjected to oxygen annealing or those grown under a higher oxygen pressure exhibit a lowered carrier density of about $(1–2)\times10^{13}$ cm^{-2} and a typical mobility of 1000 cm$^2\cdot$V$^{-1}\cdot$s^{-1} at 2 K.[9–25] The emerging consensus is that the high carrier density of 4×10^{16} cm^{-2} is due to the electrons associated with oxygen vacancies in the bulk STO substrate, and they have a three-dimensional (3D) character, while the lower carrier density of 10^{13} cm^{-2} may be an intrinsic feature of the interface. However, the origin of these intrinsic interface charge carriers is strongly debated. The prevalent interpretation relies on the polar discontinuity at the interface.[9,26] The STO terminated planes, $(Ti^{4+}O_2^{2-})^0$ and $(Sr^{2+}O^{2-})^0$, are formally neutral in the simple ionic limit, while the LAO planes, $(La^{3+}O^{2-})^+$ and $(Al^{3+}O_2^{2-})^-$, have alternating $\pm e$ charge. The charge discontinuity between $(Ti^{4+}O_2^{2-})^0/(La^{3+}O^{2-})^+$ or $(Sr^{2+}O^{2-})^0/(Al^{3+}O_2^{2-})^-$ could create a built-in potential in the growing LAO film. The accumulation of this potential to a large enough value at a certain film thickness results in an injection of carriers from the film surface into the interface, thus forming a 2DEG. In principle, the polar catastrophe can be avoided if 0.5 electron per unit cell accumulates in the interfacial TiO_2 plane. This amounts to an electron carrier density of 3.4×10^{14} cm^{-2}, approximately one order of magnitude higher than the sheet density commonly obtained. It is also notable that the experimentally detected electric field accumulated in the LAO film is much lower than the predicted value.[27] On the other hand, the polar catastrophe model is based on the assumption that the interface is chemically abrupt. Nevertheless, the ion transfer across the interface and the formation of defects have been identified to play important roles in the transport properties of the LAO/STO interfaces. For example, there is a strong evidence of La interdiffusion into STO, which can act as electron donors.[28,29] Additionally, in the growth of oxide heterostructures, the match between the anion (oxygen) sublattice rather than that between the cation sublattice is dominant. However, the possible oxygen ion redistribution across the oxide–oxide interface, which is usually associated with a strong electron redistribution on neighboring cations, is poorly understood.[30–33] For instance, although most bulk-like oxygen vacancies in STO-base heterostructures can be removed by suitable annealing, it remains unclear whether some oxygen vacancies can be stabilized at the interface by the space charge effect. These interface-stabilized oxygen vacancies, if they survive unexpectedly the annealing under high oxygen pressure, would play a nontrivial role on the interface conduction since oxygen vacancies act as one of the most effective electron donors in STO.

Another striking issue is that the carrier mobilities at oxide interfaces are significantly lower than those obtained in bulk STO materials. Specifically, the typical mobility for the intensively investigated LAO/STO interface is approximately 1000 cm$^2\cdot$V$^{-1}\cdot$s^{-1} at 2 K. This value is still much lower than those for three-dimensional oxygen-deficient STO single crystals[34] and La-doped STO epitaxial films,[8] amounting to 1.3×10^{4} cm$^2\cdot$V$^{-1}\cdot$s^{-1} and 3.2×10^{4} cm$^2\cdot$V$^{-1}\cdot$s^{-1}, respectively. Though there are reports of enhanced mobility at the LAO/STO interfaces by defect engineering,[35] it remains unclear whether the carrier mobilities are limited by the sample quality or whether they can be enhanced by different material combinations.

The mechanism that plays the dominant role in the formation of 2DEGs at polar oxide interfaces has not been unambiguously determined. The ways toward enhanced carrier mobility are also elusive, as are the needed tests of material cleanliness which must be far more sensitive than any structural or chemical characterization methods. In semiconductor 2DEGs, the achievement of high mobilities has been accompanied by the observation of hitherto unknown phenomena—first the integer quantum Hall effect (QHE),[36] and later, in even cleaner samples, the fractional quantum Hall effect (FQHE).[37] These discoveries were the subjects of the 1985 and 1998 Nobel Prizes in physics, respectively. In the progress of oxide electronics, similar phenomena have already been observed in ZnO-based oxide heterostructures.[38,39] It therefore becomes extremely interesting to investigate these fascinating physical phenomena at complex oxide interfaces with strongly-coupled d-orbital electrons, which may open new avenues for condensed matter physics. In this review, we will discuss our recent experimental work on an alternative approach to create oxide 2DEGs by interfacial redox reactions.[33] Relying on interface confined redox reactions, an oxide 2DEG with electron mobility exceeding 100000 cm$^2\cdot$V$^{-1}\cdot$s^{-1} at 2 K has been realized.[40]

2. Metallic and insulating interfaces controlled by interfacial redox reactions

To date, complex oxide 2DEGs have been realized almost exclusively in polar interfaces consisting of two perovskite-type oxides, particularly those heterostructures based on

$SrTiO_3$. Interestingly, it remains unclear why each conducting interface has to involve STO, and whether 2DEGs can be obtained when the capping film is made amorphous rather than crystalline, i.e., when the interface polarity is strongly depressed.

Motivated by the simple question of why does each 2DEG involve STO, we found that chemical redox reactions at the oxide interface provide an alternative approach to create 2DEGs.[33] Regardless of the interface polarity, when depositing certain insulating oxides with higher oxygen affinity on the STO single crystalline substrate, the overlayer can absorb oxygen from STO. This can alter the wideband insulator of stoichiometric STO into a semiconductor, metal, superconductor, or even a magnet, depending on the concentration of oxygen vacancies. For instance, such an interfacial chemical redox reaction results in a remarkable metallic interface between the amorphous LAO film and the crystalline STO substrate, a-LAO/STO, the properties of which turn out to be quite similar to those of its all-crystalline counterpart.[41–43]

The a-LAO/STO was grown by PLD at room temperature. Compared to the conventional high temperature film growth procedure, room temperature deposition has the advantage that it rules out any annealing-induced oxygen vacancies in STO substrates. Moreover, the possibility of La interdiffusion, as frequently observed in the crystalline LAO/STO sample grown at high temperatures, should be also strongly suppressed during the deposition at room temperature.

Figure 1(a) shows a high angle annular dark field (HAADF) scanning transmission electron microscopy (STEM) image of an a-LAO/STO sample.[41] A well-defined amorphous–crystalline interface is confirmed. Further measurements by electron energy loss spectroscopy (EELS) suggest that the interface is atomically sharp without significant intermixing.[41] The surface morphology of a-LAO/STO, as illustrated in Fig. 1(b), shows a flat terrace-like surface with a step height of 0.4 nm, similar to that of the STO substrate. As shown in Figs. 1(c)–1(e), the a-LAO/STO shows a metallic behavior in the investigated temperature range of 2–300 K, despite both a-LAO and STO being highly insulating themselves. The sheet carrier density n_s, which is dominated by electrons, is nearly constant in the temperature range of 100–300 K, with a value of 1.2×10^{14} cm^{-2} (Fig. 1(d)). At $T < 100$ K, n_s decreases with decreasing temperature and reaches $\sim6\times10^{13}$ cm^{-2} at 2 K. Such a partial carrier freezing-out effect upon cooling probably indicates the presence of trapped electrons with a typical activation energy of 10–20 meV as reported for amorphous $CaHfO_3$/STO interfaces.[44] The electron mobility μ_s increases upon cooling and saturates around $\sim$ 300 $cm^2\cdot V^{-1}\cdot s^{-1}$ at 2 K (Fig. 1(e)). Notably, the carrier density and the carrier mobility for the a-LAO/STO heterostructures are of the same order of magnitude as those reported for the crystalline LAO/STO deposited at high temperatures, as also shown in Figs. 1(c)–1(e).

Similar to crystalline LAO/STO interfaces, the a-LAO/STO heterostructure exhibits two characteristic properties. Firstly, the interfacial conductivity of the a-LAO/STO heterostructure exhibits a strong dependence on P_{O_2} during the

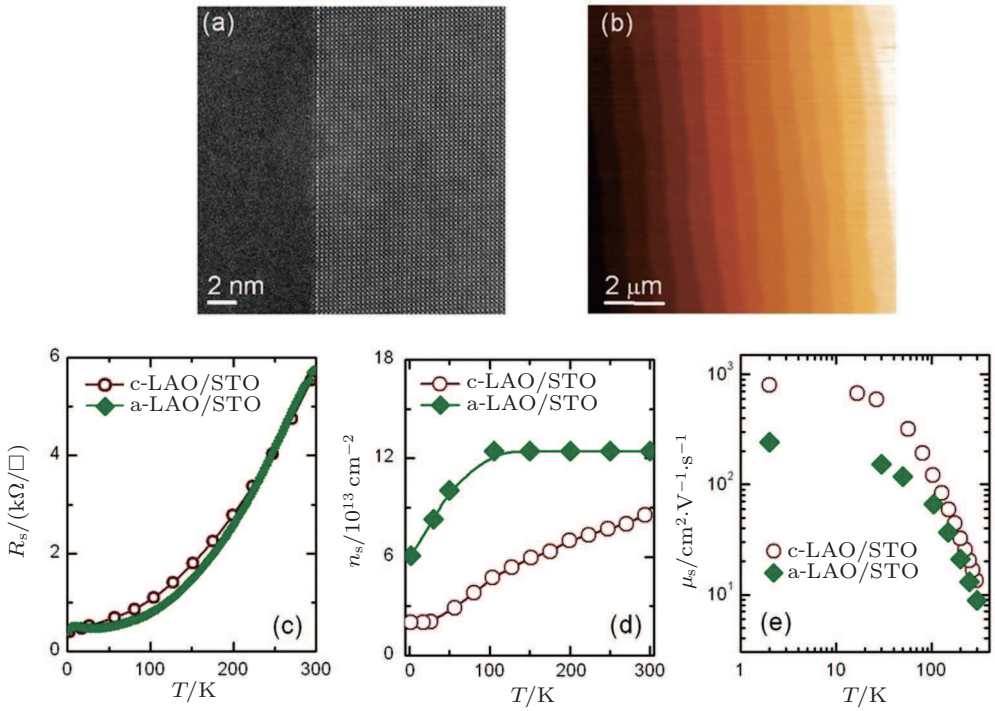

Fig. 1. Metallic conduction at the interface between amorphous $LaAlO_3$ and crystalline $SrTiO_3$ (a-LAO/STO). (a) HAADF-STEM image of the a-LAO/STO interface;[41] (b) smooth terrace-like surface of a-LAO/STO measured by atomic force microscopy; (c)–(e) sheet resistance, carrier density, and mobility as a function of temperature, respectively, for the a-LAO/STO interface deposited at 0.01 Pa. For comparison, the typical results for crystalline LAO/STO are also displayed.

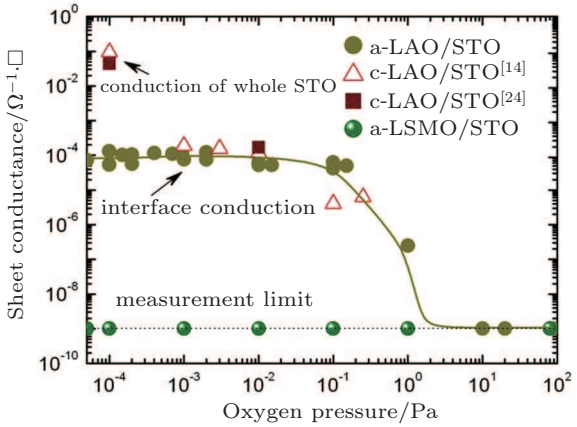

Fig. 2. Dependence of sheet conductance of a-LAO/STO on the oxygen pressure of film growth ($T = 300$ K, film thickness about 30 nm).[42] Results reported for the crystalline LAO/STO samples[14,24] are also shown for comparison.

film growth. As shown in Fig. 2, for samples with film thicknesses around 30 nm, the heterointerfaces grown at $P_{O_2} > 1$ Pa are all highly insulating, with sheet resistance R_s equal to that of the bare STO substrate ($R_s > 10^9$ Ω/□, measurement limit). Upon decreasing the pressure below 1 Pa, the a-LAO/STO heterointerface turns conductive dramatically. Note that a similar behavior has also been observed in the crystalline LAO/STO interface, except that the high temperature film growth results in a significant conductance due to the reduction of the whole STO substrate at 10^{-4} Pa.[14,24] It is also notable that the deposition of amorphous $La_{1-x}Sr_xMnO_3$ ($x = 1/8$) (a-LSMO) films on STO substrates does not result in any interfacial conductivity, even though the films are deposited in high vacuum ($P_{O_2} \leq 10^{-4}$ Pa).[33] Secondly, an interfacial metal–insulator transition that depends on the film thickness is also observed in the a-LAO/STO heterostructure, as shown in Fig. 3. For films deposited at $P_{O_2} \approx 1 \times 10^{-4}$ Pa, the a-LAO/STO heterointerfaces are insulating at $t < 1.8$ nm, while these heterointerfaces abruptly become metallic upon further increase of the film thickness. Note that the critical film thickness for the occurrence of interface conduction is nearly equal to that of c-LAO/STO ($t = 4$ uc, ~ 1.6 nm).[15] The threshold film thickness of $t \approx 1.6$ nm in c-LAO/STO has been regarded as the minimum thickness required for the occurrence of charge transfer to alleviate the polar catastrophe.[15,26] However, the polar catastrophe is absent in the amorphous–crystalline samples investigated here since there is no long-range translational symmetry in the amorphous overlayers. As will be discussed later, the critical thickness in the a-LAO/STO heterostructure may indicate the existence of a threshold concentration of oxygen vacancies at which the localized conduction regions evolve to overlap. This viewpoint is also consistent with the fact that the critical thickness for the occurrence of metallic conductivity of the a-LAO/STO heterointerface is increased upon increasing P_{O_2}.[42,43]

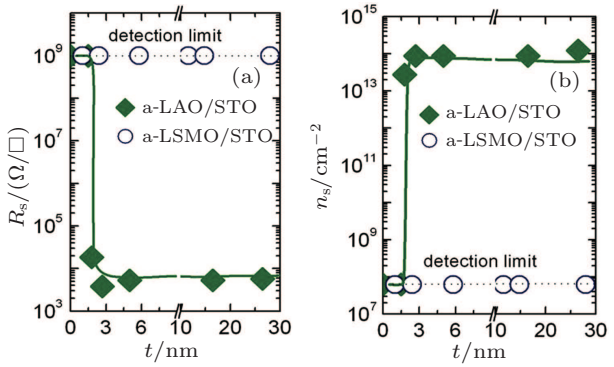

Fig. 3. Critical dependences of (a) sheet resistance and (b) carrier density of a-LAO/STO on film thickness.

In-situ X-ray photoelectron spectroscopy (XPS) measurements give a direct evidence that the conductivity of the a-LAO/STO heterointerface results from the formation of oxygen vacancies on the STO side.[33] Figures 4(a) and 4(b) show the Ti $2p_{3/2}$ spectra for a-LAO/STO of different film thicknesses grown at $P_{O_2} \approx 1 \times 10^{-4}$ Pa. As expected, no clear Ti^{3+} signal in the $2p_{3/2}$ core-level spectra could be detected in the bare STO substrate. However, a finite amount of Ti^{3+} is already present in the insulating samples, even at $t = 0.4$ nm. This suggests the formation of defects in the STO, either by intermixing or oxygen vacancies. The prominent feature of the XPS result is that the amount of Ti^{3+} increases with increasing film thickness, as shown in Fig. 4(b). This indicates that the oxygen vacancies evolve upon film deposition and thus rules out intermixing. Such a conclusion is further confirmed by the fact that annealing a-LAO/STO in high oxygen pressure decreases the Ti^{3+} signal to almost zero (Fig. 4(b)) and removes the conductivity completely.

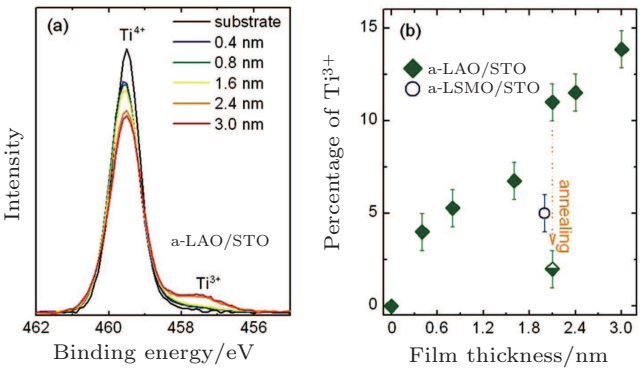

Fig. 4. (a) The Ti $2p_{3/2}$ XPS spectra for a-LAO/STO of different film thicknesses grown at $P_{O_2} \approx 1 \times 10^{-4}$ Pa. The spectra were measured at an emission angle of 80°. (b) The film thickness dependent percentage of Ti^{3+} for a-LAO/STO, where $[Ti^{3+}] + [Ti^{4+}] = 100\%$. Annealing the 2.1 nm a-LAO/STO sample at 150 °C for 1.5 h in 0.6 bar pure O_2 reduces the Ti^{3+} signal almost to zero.[33]

It has been generally argued that the oxygen vacancies are created by the bombardment due to the high energy of the arriving species during PLD process at $P_{O_2} < 0.1$ Pa.[44,45] However, this viewpoint is hardly compatible with the trend that increasing the film thickness enhances the Ti^{3+} content signifi-

cantly, as shown in Fig. 4. Furthermore, the bombardment scenario cannot explain the insulating nature of the a-LSMO/STO interface grown at $P_{O_2} \approx 1 \times 10^{-4}$ Pa. Besides their high energy, the plasma species also exhibit a high chemical reactivity at $P_{O_2} < 0.1$ Pa. Our results strongly suggest that the formation of oxygen vacancies in the a-LAO/STO heterostructure results from the outward diffusion of oxygen ions from the STO lattice due to the exposure of the STO surface to the reactive LAO plasma species with higher chemical reactivity.

In the scenario of interface redox reaction, the deposited species react with the oxygen ions (O^{2-}) present in the STO substrate. Interestingly, the defect formation energy of the TiO_2-terminated STO surface (5.94 eV), which is considerably smaller than that of the bulk,[46] is comparable to the bond dissociation energy of oxygen molecules (5.11 eV[47]). In this case, besides the oxygen source from the target and the background oxygen, oxygen ions in the STO substrates diffuse outward to oxidize the reactive plasma species absorbed on the STO surface, as schematically depicted in Fig. 5(a). It should be noted that though it has been confirmed that the STO substrate can act as an oxygen source for the oxide film growth at high temperatures,[30–32] the room temperature outward diffusion of oxygen ions from the STO substrate during the growth of oxide film by PLD has not been recognized previously. On the other hand, similar outward diffusion of oxygen ions from the STO substrate has been observed during the room-temperature growth of reactive metals of Ti and Y films by molecular beam epitaxy under ultrahigh vacuum.[48]

In the case of a metal–oxide interface, the redox reaction can be regarded as an electron transfer process from metal atoms to the Ti^{4+} accompanied with the oxygen ion reconstruction. The chemical interactions at the interface between a metal and the TiO_2 or STO surface are controlled not only by the thermodynamic stability of the metal oxide, but also by the space charge at the metal/oxide interface, which is determined by the interface electronic configuration, i.e., the relative Fermi level of the metal and that of the TiO_2 or STO before contact.[49] An interfacial redox reaction can occur at room temperature when the formation heat of metal oxide, ΔH_f^O, is lower than -250 kJ/(mol O) and the work function of the metal, φ, is in the range of 3.75 eV$< \varphi <$ 5.0 eV.[49] For oxide–oxide interfaces, both the electron transfer and the redox reaction across the interface are still poorly understood. Taking ABO_3 perovskites for example, where A is an electropositive cation such as an alkali, alkaline-earth, or rare-earth ion, the electropositive character of the A-site ion minimizes its contribution to the electronic states near the Fermi level E_F. Generally, in these oxides, the top of the valence band is primarily oxygen 2p non-bonding in character, while the conduction band arises from the π^* interaction between the B site transition metal t_{2g} orbitals and oxygen.[50–52] Therefore, the electron transfer across the perovskite-type interface is expected to depend primarily on the electronegativity and the coordination environment of the transition metal ions on the B site.

Table 1. Metallic and insulating perovskite-type interfaces based on $SrTiO_3$.

System	Interface polarity	B site reactivity	Interface conduction
$LaAlO_3$/STO[9]	√	√	√
$LaTiO_3$/STO[10]	√	√	√
$LaGaO_3$/STO[12]	√	√	√
$LaCrO_3$/STO[53]	√	×	×
$LaMnO_3$/STO[54]	√	×	×
Amorphous $LaAlO_3$/STO[33]	×	√	√
Amorphous $CaHfO_3$/STO[44]	×	√	√
Amorphous STO/STO[33]	×	√	√
Amorphous LSMO/STO[33]	×	×	×

Table 1 summarizes most of the STO-based perovskite oxide interfaces reported so far. Besides LAO/STO, $LaTiO_3$/STO[10] and $LaGaO_3$/STO[12] are the other two most researched crystalline systems that show metallic interfaces with STO. Additionally, the crystalline $LaCrO_3$/STO[53] interface is very interesting since it shows an interface polarity while exhibiting an insulating behavior. As for the amorphous STO-based heterointerfaces, besides the metallic a-LAO/STO, amorphous $CaHfO_3$/STO[44] and amorphous STO/STO[33] are the other systems that show metallic interfaces. Additionally, the $La_{1-x}Sr_xMnO_3$/STO interface is another notable system. The undoped $LaMnO_3$ is polar, however it forms an insulating interface with STO.[54] On the other hand, although most crystalline $La_{1-x}Sr_xMnO_3$ samples are conductive,[55] their amorphous forms are insulating and form insulating interfaces with STO.[33] Remarkably, the B-site metals for most conductive perovskite-type interfaces, Al, Ti, and Hf, each satisfy well the criterion for metal–oxide interface redox reactions: $\Delta H_f^O < -250$ kJ/(mol O) and 3.75 eV$< \varphi <$ 5.0 eV. On the other hand, Mn, Cr, and Ga, the main atomic components of the corresponding $La_{1-x}Sr_xMnO_3$, $LaCrO_3$, and $LaGaO_3$ plasmas, locate on the border region for the occurrence/nonoccurrence of redox reaction of metals on the TiO_2 surface at room temperature.[49] Though the redox reactions at oxide–oxide interfaces could be more complex than those at metal–oxide interfaces, the lack of interface redox reactions should explain the insulating nature of the $LaCrO_3$/STO and the $La_{1-x}Sr_xMnO_3$/STO interfaces. As illustrated in Fig. 5(b), for the ABO_3/STO (A = La) perovskite-type interfaces, compared to the interface polarity viewpoint, it is surprising to find that the redox reaction scenario can better account for most of the metallic and insulating interfaces reported so far. Moreover, in metallic perovskite interfaces, the B-site metals locate mainly in the region of $\Delta H_f^O < -350$ kJ/(mol O) and 3.75 eV$< \varphi <$ 4.4 eV.

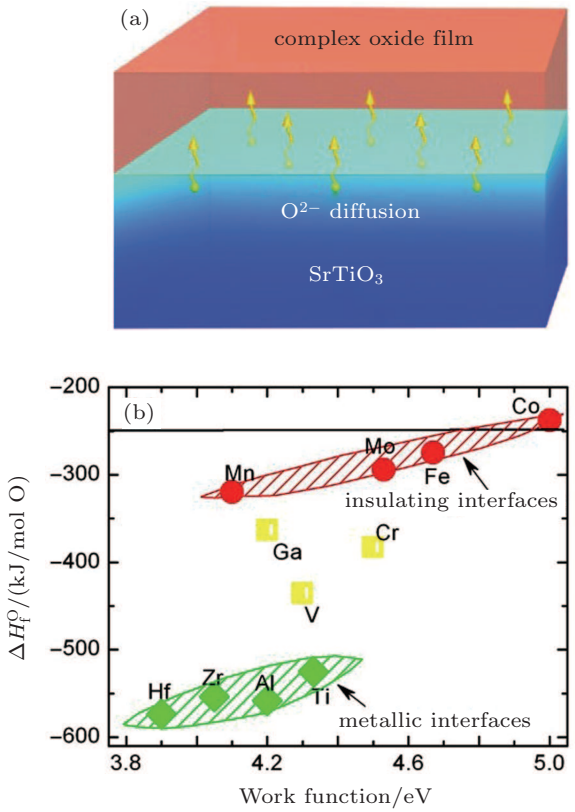

Fig. 5. (a) Sketch diagram of redox reaction at oxide interfaces;[33] (b) formation heat of metal oxides versus the work function of *B*-site metals for the ABO_3/STO (A = La) perovskite-type interfaces. For metallic interfaces, the *B*-site metals locate mainly in the region of $\Delta H_f^O < -350$ kJ/(mol O) and 3.75 eV$< \varphi <$ 4.4 eV (squares and diamonds). The solid line indicates the border of the redox reaction for metals on the STO surface.

Complying with the redox reaction mechanism, other Al-containing oxides have also been used to create an oxide 2DEG with STO as demonstrated by atomic layer deposition or electron beam evaporation.[56,57] It is also notable that the most recent research reveals that Al excess is necessary to assure a metallic interface for c-LAO/STO,[58] which further highlights the importance of the interface redox reaction for the formation of 2DEG at the LAO/STO interface. By using the concept of interfacial redox reaction, many new opportunities to tune the interface conduction have also been demonstrated. For example, by improving the chemical reactivity of the plasma plume through deposition the LAO film in argon rather than in oxygen, the a-LAO/STO conduction can be enhanced.[59] Moreover, the conductivity of the a-LAO/STO interface is also found to be modified by an external electric field provided *in-situ* through a biased truncated cone electrode (-10 V$\leq V_{\rm bias} \leq 20$ V) during film deposition.[60,61] By modulating the charge balance of the plasma plume, a substantial surface charge is found to build up transiently during the initial stage of the film growth when the truncated cone electrode is biased. The presence of this surface potential is expected to greatly influence the surface/plasma interaction. More specifically, experimental observations seem consistent with a lowering of the incoming Al-ion flux by the applied bias, which shifts the interfacial conduction of a-LAO/STO from metallic over semiconducting to an insulating transport mode. This remarkable behavior further indicates the importance of the Al-ion flux on the amount of near-interface oxygen vacancies formed at the STO surface and therefore the interface conduction.

3. High-mobility 2DEG at the spinel/perovskite interface of γ-Al_2O_3/$SrTiO_3$

In the above section, it has been demonstrated that the redox reaction at oxide interfaces provides a new approach to design metallic and insulating interfaces. However, confining the oxygen vacancies at the interface to realize 2DEGs is still rather challenging, since the high quality epitaxial oxide heterostructures are normally formed at high temperatures, such as at 600 °C. At such a high temperature, oxygen diffuses over many micrometers in minutes because STO is a mixed conductor at high temperatures. This would completely level out any nanometer-scale steps in the oxygen concentration profiles of the STO-based heterostructures. In this vein, spatially confined redox reactions at the oxide interfaces turn out to be a crucial issue to realize high mobility 2DEGs. Fortunately, the defect-chemistry research into STO implies a positive space charge core at its grain boundary, which is expected to result in the accumulation of electrons in proximity to the interface.[62,63] This makes the concept of interface-stabilized oxygen vacancies highly practicable, particularly at an atomically engineered oxide interface. Recently, we realized such interface confined oxygen vacancies at an epitaxial spinel-perovskite interface between γ-Al_2O_3 (GAO) and STO.[40] Remarkably, this new type of oxide 2DEG shows a record electron mobility greater than 140000 $cm^2 \cdot V^{-1} \cdot s^{-1}$ at 2 K, 100 times higher than that typically obtained in the perovskite-type oxide interfaces studied so far.

The most intensively investigated oxide interfaces for 2DEGs are Al-containing perovskites grown on STO, such as the LAO/STO. Since Al satisfies the criteria for redox reactions on the STO surface, any Al-containing oxide has the possibility to exhibit a metallic interface with STO. Figure 6 summarizes the lattice parameters for most Al-based oxides. Each of the relevant perovskite compounds shows a smaller lattice parameter than that of STO ($a_{\rm STO} = 0.3905$ nm) with a lattice mismatch exceeding 3.2% (for LAO/STO). Extending the lattice parameter range upward beyond that of STO, one has to rely on the oxides with a spinel structure, the lattice parameters of which are normally larger than 0.4 nm ($a/2$). It is noteworthy that the GAO is distinguished from the other oxides by an excellent lattice match with STO ($a_{\rm GAO} = 0.7911$ nm, lattice mismatch of 1.2%).[64] As shown in Figs. 7(a) and 7(b), despite differences in cation sublattices, the oxygen sublattices

of perovskite STO match perfectly with the oxygen sublattices of spinel GAO. This makes it possible to grow epitaxially GAO/STO spinel/perovskite heterostructures in a persistent two-dimensional layer-by-layer mode as confirmed by the periodic oscillations of the RHEED intensity during film growth (Fig. 7(d)). Note that for the GAO films grown along the (001) direction, one RHEED intensity oscillation corresponds to the growth of one quarter unit cell film, since the GAO unit cell consists of four neutral AlO_x sub-unit cells with an interlayer distance of about 0.2 nm. Under optimized conditions, persistent sub-unit-cell layer-by-layer growth is observed till more than 200 RHEED oscillations. The obtained GAO/STO heterostructure shows a perfect terrace surface with a terrace height of 0.4 nm, as determined by atomic force microscopy (Fig. 7(e)). As shown in Figs. 7(f) and 7(g), STEM-EELS measurements confirm a well-defined cubic-on-cubic coherent heterointerface with no obvious dislocations.

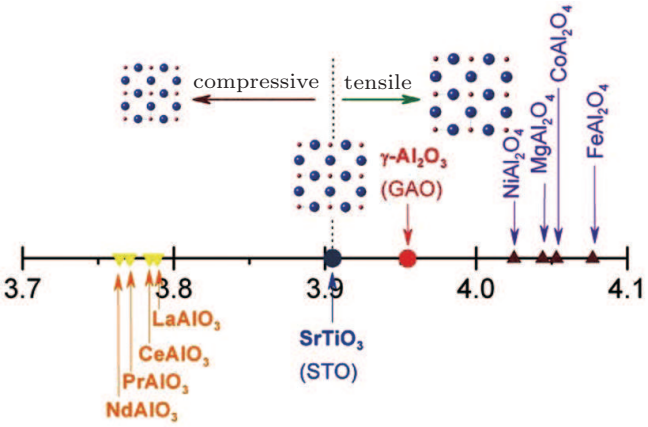

Fig. 6. Lattice parameter diagram for most Al-based oxides that show lattice parameters close to that of STO ($a_{STO} = 3.905$ Å).

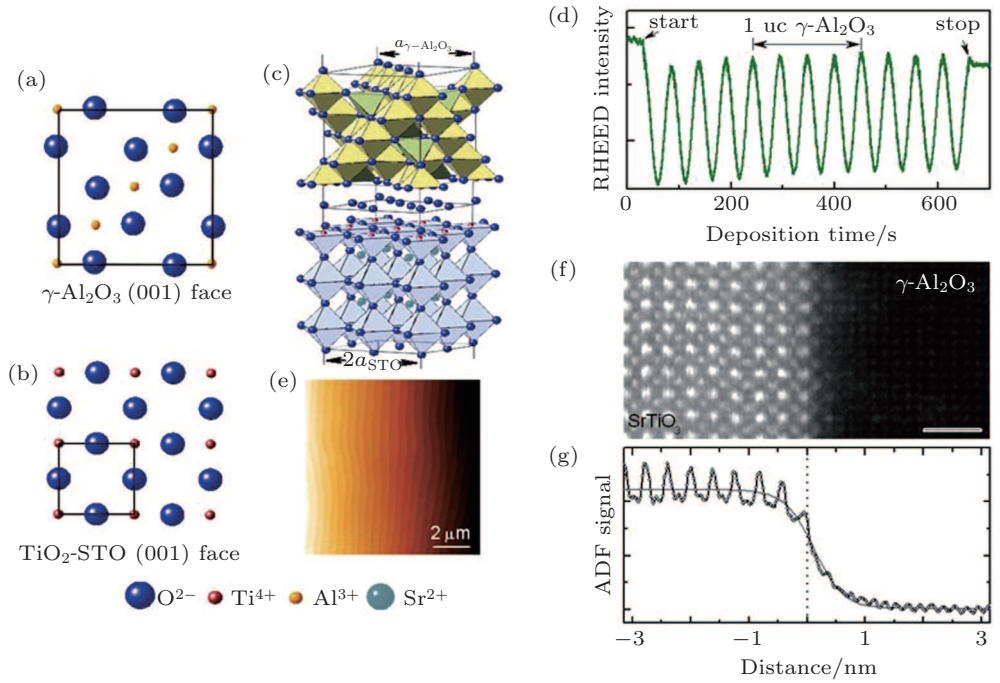

Fig. 7. The epitaxial spinel/perovskite GAO/STO interfaces. (a) and (b) The compatibility in oxygen sublattices of a GAO surface and the TiO_2-terminated STO surface, which forms the backbone to build the spinel/perovskite heterostructure as illustrated in panel (c). (d) Typical RHEED intensity oscillations for the growth of a 3-uc GAO on STO in a sub-unit-cell layer-by-layer mode. (e) A 10 μm×10 μm AFM morphology of GAO/STO. (f) High-angle annular dark field STEM image of the epitaxial GAO/STO interface, the scale bar is 1 nm. Sr ions are the brightest, followed by Ti. The faintly visible Al elements can be determined by the averaged line profiles across the interface shown in panel (g). A well developed TiO_2-AlO_x heterointerface is defined.[40]

Similar to the LAO/STO interface, the GAO/STO heterostructure can exhibit a metallic interface between the two insulators with electrons as the dominant charge carriers. Strikingly, 2DEGs with extremely high Hall electron mobilities can be obtained at this spinel/perovskite interface when the GAO film is grown at an oxygen background pressure of 0.01 Pa and a growth temperature of 600 °C. As shown in Fig. 8, the interfacial conduction depends critically on the thickness, t, of the GAO film. The interface conduction occurs only when $t \geq 2$ uc. By carefully controlling the film growth down to a sub-unit-cell level, a great decrease in R_s of approximately four orders in magnitude upon cooling is observed at $t = 2.5$ uc (Fig. 8(a)). Furthermore, the low-field Hall measurements show an impressive Hall mobility of approximately 1.4×10^5 cm$^2\cdot$V$^{-1}\cdot$s^{-1} and a carrier density of 3.7×10^{14} cm^{-2} at 2 K (Figs. 8(b) and 8(c)). Note that the carrier density of the GAO/STO varies dramatically in the range of 10^{13}–10^{15} cm^{-2} with respect to the film thickness and the high mobilities of

$\mu_{\rm Hall} \geq 10^4$ cm^2·V^{-1}·s^{-1} at $T = 2$ K are only detected in the thickness range of 2 uc $\leq t <$ 3 uc. Further increasing t deteriorates the electron mobility to less than 1000 cm^2·V^{-1}·s^{-1}, probably due to the significant outward diffusion of the Ti cations across the interface as observed by electron energy loss spectroscopy.[40]

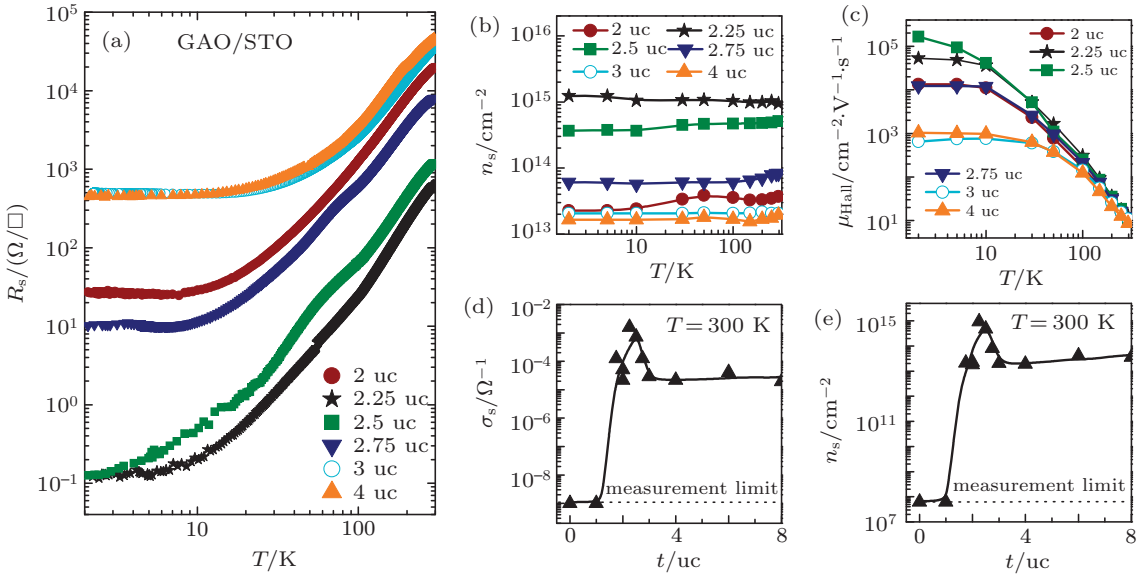

Fig. 8. Thickness-dependent transport properties of the GAO/STO interface. (a)–(c) Temperature dependences of sheet resistance R_s, carrier density n_s, and low-field electron Hall mobility $\mu_{\rm Hall}$ for the interface conduction at different film thicknesses. (d) and (e) Thickness dependences of the sheet conductance σ_s and n_s measured at 300 K. High-mobility 2DEGs are obtained in the thickness range of 2 uc $\leq t <$ 3 uc.[40]

The high mobility 2DEG at the GAO/STO interface exhibits unambiguous angle-dependent Shubnikov–de Haas (SdH) quantum oscillations, which are superimposed on a huge background of positive magnetoresistance (Fig. 9(a)). After subtracting the magnetoresistance background, the SdH oscillations become apparent, as shown in Fig. 9(b). The extrema positions show a cosine dependence on the angle θ between the magnetic field and the surface normal (Fig. 9(c)). This reveals the two-dimensional nature of the electron gas formed at the GAO/STO interface. Besides, the absence of oscillations at $\theta = 90°$ further confirms that the spatial width of the 2DEG is at least smaller than the cyclotron radius at 15 T, the typical value of which is below 10 nm for GAO/STO heterostructures. Moreover, the angular dependence of the SdH oscillations measured at high magnetic fields suggests a multiple-subband contribution to the charge transport. For instance, an extra feature is observed at $\theta = 50°$ with $B\cos\theta = 7.2$ T, which may result from a π shift of the oscillations due to a spin-split band. Such a phase shift has been observed in the high-mobility 2DEG of the GaN/AlGaN interface when the Zeeman energy (depending on the total B) and the cyclotron energy (depending on the perpendicular component of B) are equal.[65] Importantly, the low-field dependence of the SdH oscillations reveals the typical behavior due to a single band.[40] More quantitative analysis of the temperature dependent SdH oscillations leads to a carrier effective mass of $m^* = (1.22 \pm 0.03)m_e$ (m_e is the bare electron mass), consistent with that reported for the LAO/STO heterostructures.[25,66] Furthermore, the total scattering time τ for the GAO/STO interface is determined to be $\tau = 4.96 \times 10^{-12}$ s, corresponding to a quantum mobility $\mu_{\rm SdH} = e\tau/m^*$ of 7.2×10^3 cm^2·V^{-1}·s^{-1}. This unprecedented high $\mu_{\rm SdH}$ in our GAO/STO 2DEG is more than one order of magnitude higher than that observed in the perovskite-type LAO/STO[25,66] and $GaTiO_3$/STO[67] heterostructures, which is typically below 300 cm^2·V^{-1}·s^{-1}. Note that the difference between $\mu_{\rm Hall}$ and $\mu_{\rm SdH}$ could come from a difference in scattering time (i.e., the transport scattering time and the total scattering time, respectively). SdH oscillations also represent a direct measurement of the area of the Fermi surface. For the GAO/STO, the typical Fermi cross-section corresponds to a SdH frequency of $F = 14.7$ T. By taking a single valley and the spin degeneracy $g_s = 2$, this gives $n_{\rm 2D} = 7.1 \times 10^{11}$ cm^{-2}, assuming a circular section of the Fermi surface. As a consequence, the sheet carrier density deduced from the SdH oscillations shows a significant discrepancy with that obtained from the Hall measurements. This is probably due to the existence of low mobility 2D or 3D subband electrons, which do not satisfy the conditions to exhibit SdH oscillations ($\hbar\omega_c \geq k_B T$ and $\omega_c\tau \geq 1$) but contribute nevertheless to the Hall signal. For $n_{\rm 2D} = 7.1 \times 10^{11}$ cm^{-2}, the corresponding Fermi wavelength $\lambda_F = 2\pi/k_F = \sqrt{2\pi/n}$ is about 30 nm. The mean free path $l_{\rm mfp}$ of these electrons

with $\tau = 4.96 \times 10^{-12}$ s and $m^* = 1.22m_e$ is approximately 100 nm, which is approximately 10 times larger than the l_{mfp} for the LAO/STO interfaces.[1]

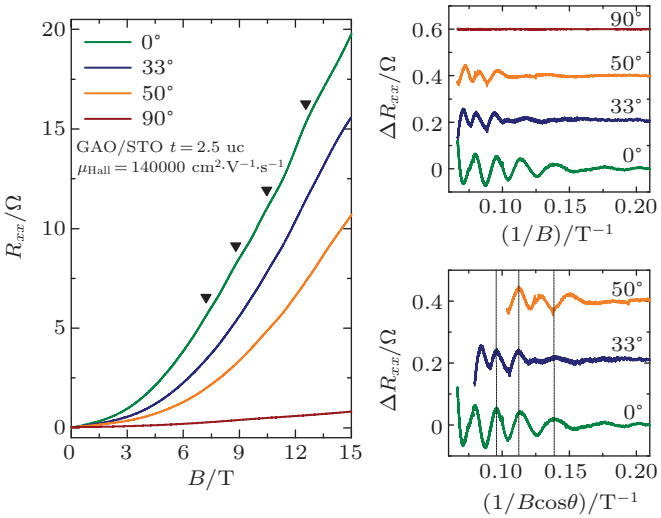

Fig. 9. Two-dimensional quantum oscillations of conduction at GAO/STO interfaces. (a) Longitudinal resistance R_{xx} as a function of magnetic field with visible SdH oscillations (arrowheads) under different tilt angles θ at 0.3 K for the $t = 2.5$ uc sample. (b) and (c) Amplitudes of the SdH oscillations, ΔR_{xx}, under different θ versus the reciprocal total magnetic field and the reciprocal perpendicular magnetic field component, respectively. The SdH oscillations depend mainly on the reciprocal perpendicular magnetic field component, particularly in the θ angle range of 0°–33°, which suggests the GAO/STO interface has a two-dimensional conduction nature.[40]

To determine the origin and the depth profile for the conduction in the GAO/STO heterostructure, angle resolved XPS measurements are also performed. We find that the electrons are exclusively accumulated on the otherwise empty 3d shell of Ti^{4+} on the STO side. The most prominent feature of the XPS data is that the Ti^{3+} signal in the GAO/STO heterointerface shows a strong dependence on the photoelectron detection angle α with respect to the surface normal. An increase of the Ti^{3+} signal with increasing α, as shown in Fig. 10(a), is clearly detected for $t = 2.5$ uc with the highest Hall mobility. This further confirms that the conduction in our GAO/STO heterointerface is highly confined at the interface region. To make furhter quantitative analyses, we assume a simple case that the 2DEG extends from the interface to a depth d into the STO substrate.[68] The interface region is further assumed to be stoichiometric, sharp, and characterized by a constant fraction p of Ti^{3+} per STO unit cell. By taking into account the attenuation length of photoelectrons, the best fitting of the experimental $I(Ti^{3+})/I(Ti^{4+})$ ratios gives $p \approx 0.31$, which corresponds to $n_s \approx 2.1 \times 10^{14}$ cm^{-2} and $d = 0.9$ nm. Therefore, the electrons at our GAO/STO heterointerface are strongly confined within approximately the first 2 uc of the STO surface proximate to the interface. Note that the n_s deduced here is slightly lower than that obtained from the Hall data (Fig. 8(c)). This could be due to the outward diffusion of the Ti cations into alumina films, where Ti^{4+} is the dominant component.

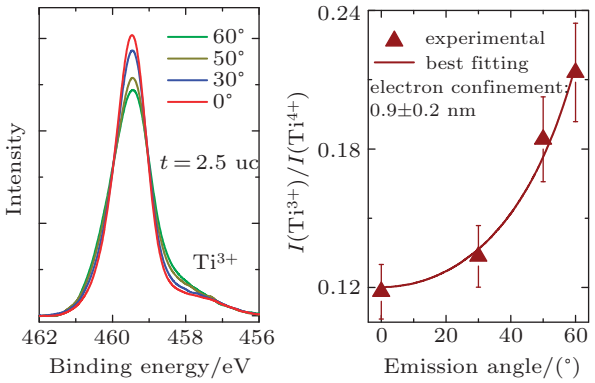

Fig. 10. Spatial confinement of the 2DEG at the GAO/STO heterointerface determined by angle-resolved XPS. (a) The Ti $2p_{3/2}$ XPS spectra at various emission angles α for the $t = 2.5$ uc sample; (b) The angle dependence of the ratio of Ti^{3+} to Ti^{4+} signal, $I(Ti^{3+})/I(Ti^{4+})$, indicates a strong confinement of the conduction layer within 0.9 nm. Error bars indicate standard deviations, ±20%, for experimental values.[40]

The presence of Ti^{3+} implies the formation of oxygen vacancies on the STO side. This scenario is consistent with the fact that the interfacial conductivity can be completely removed when the Ti^{3+} content is significantly suppressed by annealing the sample in 1 bar pure O_2 at a temperature higher than 200 °C. Such an oxygen-vacancy-dominated 2DEG is expected to be formed as a consequence of chemical redox reactions occurring on the STO surface during the film growth of GAO, analogous to what has been observed in amorphous STO-based heterostructures grown at room temperature.[33] Note that the 2DEG at the crystalline GAO/STO heterointerface is formed at a high temperature of 600 °C, where oxygen ions in the STO are already highly mobile. This is normally expected to level out any difference in the depth profile of oxygen distribution in the STO, as discussed previously. However, this is not the case in the crystalline GAO/STO heterostructures as inferred from both Figs. 9 and 10. Moreover, the conduction at the interfaces of thick films, for example at $t = 8$ uc, can survive annealing at 300 °C for 24 h in 1 bar pure O_2 with only negligible changes in conductivity.[40] These features strongly suggest that the oxygen vacancies and the 2DEGs are stabilized by an interface effect, for instance, the formation of a space charge region near the heterointerface, as illustrated in Fig. 11.[62,63] In the scenario of space charge induced formation of 2DEGs, oxygen vacancies are enriched at the space charge core, while electrons are located in a separate space charge layer parallel to the surface. This is similar to the situation of the modulation doping observed in semiconductor 2DEGs[69] and may explain the extremely high mobility observed in the GAO/STO interface. It is worth noting that an inherent oxygen ion deficiency has been observed at the grain boundary of STO bicrystals,[70] where a considerable electron accumulation has also been predicted if the barrier height of the grain boundary is deliberately controlled.[63] The high electron mobility of STO-based oxide materials at low temperatures is generally related to the polarization shielding

of the ionized defect scattering centers driven by the large dielectric constant of the STO.[71] The higher mobility of our spinel/perovskite oxide interface compared to that of the perovskite-type oxide heterointerface may also be due to the better lattice match and thereby a more perfect structure and a well-defined interface.

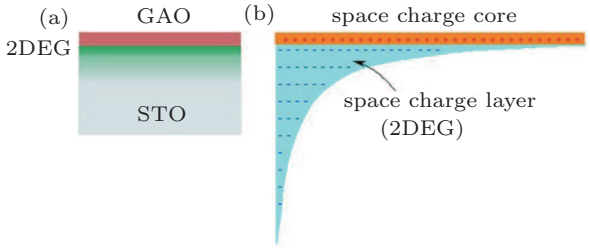

Fig. 11. Space charge layer dominated 2DEG at the GAO/STO heterointerface.

4. Conclusions and outlook

We have reviewed our recent experimental work on 2DEGs at oxide interfaces. Besides the interface polarity, the interfacial redox reaction at oxide interfaces provides an alternative approach to explore oxide 2DEGs. Interestingly, the a-LAO/STO system is found to show tunable metal–insulator transitions with gated electric field,[72] analogous to what has been found in the crystalline LAO/STO interface.[15] This makes the a-LAO/STO system rather promising for oxide electronics, though enhancing its carrier mobility remains challenging. On the other hand, relying on interface-confined oxygen vacancies and combining two of the largest groups of oxides, the 2DEG at the spinel/perovskite GAO/STO interface is expected to hold plenty of new physical properties, for instance, interfacial magnetism[14] and superconductivity[13] as observed in the perovskite-type LAO/STO interface. Moreover, with a large enhancement of the electron mobility, the GAO/STO heterointerface enables the design of mesoscopic quantum devices based on complex oxide 2DEGs and opens new avenues for oxide nanoelectronics and mesoscopic physics.

Acknowledgment

The authors wish to express their thanks for the collaborations and discussion with A. J. H. M. Rijnders, G. Koster, J. E. Kleibeuker, F. Trier, D. V. Christensen, N. Bovet, N. H. Andersen, T. Kasama, W. Zhang, L. Lu, F. M. Qu, R. Giraud, J. Dufouleur, B. Buchner, T. S. Jespersen, J. Nygård, E. Stamate, S. Amoruso, J. Fleig, F. W. Poulsen, and N. Bonanos.

References

[1] Mannhart J and Schlom D G 2010 *Science* **327** 1607
[2] Mannhart J, Blank D H A, Hwang H Y, Millis A J and Triscone J M 2008 *MRS Bull.* **33** 1027
[3] Kawasaki M, Takahashi K, Maeda T, Tsuchiya R, Shinohara M, Ishiyama O, Yonezawa T, Yoshimoto M and Koinuma H 1994 *Science* **266** 1540
[4] Koster G, Kropman B L, Rijnders G J H M, Blank D H A and Rogalla H 1998 *Appl. Phys. Lett.* **73** 2920
[5] Rijnders G J H M, Koster G, Blank D H A and Rogalla H 1997 *Appl. Phys. Lett.* **70** 1888
[6] Chen Y Z and Pryds N 2011 *Thin Solid Films* **519** 6330
[7] Schlom D G, Chen L Q, Pan X Q, Schmehl A and Zurbuchen M A 2008 *J. Am. Ceram. Soc.* **91** 2429
[8] Son J W, Moetakef P, Jalan B, Bierwagen O, Wright N J, Engel-Herbert R and Stemmer S 2010 *Nat. Mater.* **9** 482
[9] Ohtomo A and Hwang H Y 2004 *Nature* **427** 423
[10] Biscaras J, Bergeal N, Kushwaha A, Wolf T, Rastogi A, Budhani R C and Lesueur J 2010 *Nat. Commun.* **1** 89
[11] Moetakef P, Cain T A, Ouellette D G, Zhang J Y, Klenov D O, Janotti A, Van de Walle C G, Rajan S, Allen S J and Stemmer S 2011 *Appl. Phys. Lett.* **99** 232116
[12] Perna P, Maccariello D, Radovic M, Scotti di U, Pallecchi I, Codda M, Marré D, Cantoni C, Gazquez J, Varela M, Pennycook S J and Miletto Granozio F 2010 *Appl. Phys. Lett.* **97** 152111
[13] Reyren N, Thiel S, Caviglia A D, Fitting Kourkoutis L, Hammerl G, Richter C, Schneider C W, Kopp T, Ruetschi A S, Jaccard D, Gabay M, Muller D A, Triscone J M and Mannhart J 2007 *Science* **317** 1196
[14] Brinkman A, Huijben M, Van Zalk M, Huijben J, Zeitler U, Maan J C, Van der Wiel W G, Rijnders G, Blank D H A and Hilgenkamp H 2007 *Nat. Mater.* **6** 493
[15] Thiel S, Hammerl G, Schmehl A, Schneider C and Mannhart J 2006 *Science* **313** 1942
[16] Cen C, Thiel S, Hammerl G, Schneider C W, Andersen K E, Hellberg C S, Mannhart J and Levy J 2008 *Nat. Mater.* **7** 298
[17] Chen Y Z, Zhao J L, Sun J R, Pryds N and Shen B G 2010 *Appl. Phys. Lett.* **97** 123102
[18] Chambers S A 2011 *Surface Science* **605** 1133
[19] Park J W, Bogorin D F, Cen C, Felker D A, Zhang Y, Nelson C T, Bark C W, Folkman C M, Pan X Q, Rzchowski M S, Levy J and Eom C B 2010 *Nat. Commun.* **1** 94
[20] Pentcheva R, Arras R, Otte K, Ruiz V G and Pickett W E 2012 *Phil. Trans. R. Soc. A* **370** 4904
[21] Pavlenko N, Kopp T, Tsymbal E Y, Mannhart J and Sawatzky G A 2012 *Phys. Rev. B* **86** 064431
[22] Zhong Z C, Xu P X and Kelly P J 2010 *Phys. Rev. B* **82** 165127
[23] Herranz G, Basletić M, Bibes M, Carrétéro C, Tafra E, Jacquet E, Bouzehouane K, Deranlot C, Hamzić A, Broto J M, Barthélémy A and Fert A 2007 *Phys. Rev. Lett.* **98** 216803
[24] Kalabukhov A, Gunnarsson R, Borjesson J, Olsson E, Claeson T and Winkler D 2007 *Phys. Rev. B* **75** 121404
[25] Caviglia A D, Gariglio S, Cancellieri C, Sacepe B, Fete A, Reyren N, Gabay M, Morpurgo A F and Triscone J M 2010 *Phys. Rev. Lett.* **105** 236802
[26] Reinle-Schmitt M L, Cancellieri C, Li D, Fontaine D, Medarde M, Pomjakushina E, Schneider C W, Gariglio S, Ghosez Ph, Triscone J M and Willmott P R 2012 *Nat. Commun.* **3** 932
[27] Segal Y, Ngai J H, Reiner J W, Walker F J and Ahn C H 2009 *Phys. Rev. B* **80** 241107
[28] Willmott P R, Pauli S A, Herger R, Schlepütz C M, Martoccia D, Patterson B D, Delley B, Clarke R, Kumah D, Cionca C and Yacoby Y 2007 *Phys. Rev. Lett.* **99** 155502
[29] Chambers S A, Engelhard M H, Shutthanandan V, Zhu Z, Droubay T C, Qiao L, Sushko P V, Feng T, Lee H D, Gustafsson T, Garfunkel E, Shah A B, Zuo J M and Ramasse Q M 2010 *Surf. Sci. Rep.* **65** 317
[30] Schneider C W, Esposito M, Marozau I, Conder K, Doebeli M, Hu Y, Mallepell M, Wokaun A and Lippert T 2010 *Appl. Phys. Lett.* **97** 192107
[31] Uedono A, Shimayama K, Kiyohara M, Chen Z Q and Yamabe K 2002 *J. Appl. Phys.* **92** 2697
[32] Scullin M L, Ravichandran J, Yu C, Huijben M, Seidel J, Majumdar A and Ramesh R 2010 *Acta Mater.* **58** 457
[33] Chen Y Z, Pryds N, Kleibeuker J E, Sun J R, Stamate E, Koster G, Shen B G, Rijnders G and Linderoth S 2011 *Nano. Lett.* **11** 3774
[34] Frederikse H P R and Hosler W R 1967 *Phys. Rev.* **161** 822

[35] Huijben M, Koster G, Kruize M K, Wenderich S, Verbeeck J, Bals S, Slooten E, Shi B, Molegraaf H J A, Kleibeuker J E, Aert S V, Goedkoop J B, Brinkman A, Blank D H A, Golden M S, Tendeloo G V, Hilgenkamp H and Rijnders G 2013 *Adv. Func. Mater.*

[36] Klitzing K V, Dorda G and Peper M 1980 *Phys. Rev. Lett.* **45** 494

[37] Tsui D C, Stormer H L and Gossard A C 1982 *Phys. Rev. Lett.* **48** 1559

[38] Tsukazaki A, Ohtomo A, Kita T, Ohno Y, Ohno H and Kawasaki M 2007 *Science* **315** 1388

[39] Tsukazaki A, Akasaka S, Nakahara K, Ohno Y, Ohno H, Maryenko D, Ohtomo A and Kawasaki M 2010 *Nat. Mater.* **9** 889

[40] Chen Y Z, Bovet N, Trier F, Christensen D V, Qu F M, Andersen N H, Kasama T, Zhang W, Giraud R, Dufouleur J, Jespersen T S, Sun J R, Smith A, Nygård J, Lu L, Büchner B, Shen B G, Linderoth S and Pryds N 2013 *Nat. Commun.* **4** 1371

[41] Kleibeuker J E 2012 (Ph. D. thesis) (The Netherlands: University of Twente)

[42] Chen Y Z, Christensen D V, Trier F, Pryds N, Smith A and Linderoth S 2012 *Appl. Surf. Sci.* **258** 9242

[43] Liu Z Q, Li C J, Lü W M, Huang, X H, Huang Z, Zeng S W, Qiu X P, Huang L S, Annadi A, Chen J S, Coey J M D, Venkatesan T and Ariando 2013 *Phys. Rev. X* **3** 021010

[44] Shibuya K, Ohnishi T, Lippmaa M and Oshima M 2007 *Appl. Phys.Lett.* **91** 232106

[45] Siemons W, Koster G, Yamamoto H, Harrison W A, Lucovsky G, Geballe T H, Blank D H A and Beasley M R 2007 *Phys. Rev. Lett.* **98** 196802

[46] Carrasco J, Illas F, Lopez N, Kotomin E A, Zhukovskii Yu F, Evarestov R A, Mastrikov Yu A, Piskunov S and Maier J 2006 *Phys. Rev. B* **73** 064106

[47] Gupta A 1993 *J. Appl. Phys.* **73** 7877

[48] Hill D M, Meyer H M and Weaver J H 1989 *J. Appl. Phys.* **65** 4943

[49] Fu Q and Wagner T 2007 *Surf. Sci. Rep.* **62** 431

[50] Eng H W, Barnes P W, Auer B M and Woodward P M 2003 *J. Solid. Stat. Chem.* **175** 94

[51] Arima T, Tokura Y and Torrance J B 1993 *Phys. Rev. B* **48** 17006

[52] Zaanen J, Sawatzky G A and Allen J W 1985 *Phys. Rev. Lett.* **55** 418

[53] Chambers S A, Qiao L, Droubay T C, Kaspar T C, Arey B W and Sushko P V 2011 *Phys. Rev. Lett.* **107** 206802

[54] Boikov Yu A, Serenkov I T, Sakharov V I, Kalabukhov A S, Aurino P P, Winkler D and Claeson T 2013 *Europhys. Lett.* **102** 56003

[55] Chen Y Z, Sun J R, Wei A D, Liang S, Lv W M and Shen B G 2008 *Appl. Phys. Lett.* **93** 152515

[56] Lee S W, Liu Y Q, Heo J and Gordon R G 2012 *Nano. Lett.* **12** 4775

[57] Delahaye J and Grenet T 2012 *J. Phys. D: Appl. Phys.* **45** 315301

[58] Breckenfeld E, Bronn N, Karthik J, Damodaran A R, Lee S, Mason N and Martin L W 2013 *Phys. Rev. Lett.* **110** 196804

[59] Sambri A, Christensen D V, Trier F, Chen Y Z, Amoruso S, Pryds N, Bruzzese R and Wang X 2012 *Appl. Phys. Lett.* **100** 231605

[60] Chen Y Z, Stamate E, Pryds N, Sun J R, Shen B G and Linderoth S 2011 *Appl. Phys. Lett.* **98** 232105

[61] Trier F, Amoruso S, Christensen D V, Sambri A, Chen Y Z, Wang X, Stamate E, Bruzzese R and Pryds N 2013 *Appl. Phys. Lett.* **103** 031607

[62] Denk I, Claus J and Maier J 1997 *J. Electrochem. Soc.* **144** 3526

[63] Vollmann M, Hagenbeck R and Waser R 1997 *J. Am. Ceram. Soc.* **80** 2301

[64] Zhou R S and Snyder R L 1991 *Acta Cryst. B* **47** 617

[65] KnapW, Fal'ko V I Frayssinet E, P Lorenzini P, Grandjean N, Maude D, Karczewski G, Brandt B L, Łusakowski J, Grzegory I, Leszczyński M, Prystawko P, Skierbiszewski C, Porowski S, Hu X, Simin G, Khan M A and Shur M S 2004 *J. Phys.: Condens. Matter* **16** 3421

[66] Ben Shalom M, Ron A, Palevski A and Dagan Y 2010 *Phys. Rev. Lett.* **105** 206401

[67] Moetakef P, Ouellette D G, Williams J R, James Allen S, Balents L, Goldhaber-Gordon D and Stemmer S 2012 *Appl. Phys. Lett.* **101** 151604

[68] Sing M, Berner G, Gob K, Müller A, Ruff A, Wetscherek A, Thiel S, Mannhart J, Pauli S A, Schneider C W, Willmott P R, Gorgoi M, Schäfers F and Claessen R 2009 *Phys. Rev. Lett.* **102** 176805

[69] Dingle R, Störmer H L, Gossard A C and Wiegmann W 1978 *Appl. Phys. Lett.* **33** 665

[70] Jia C L and Urban K 2004 *Science* **303** 2001

[71] Tufte O N and Chapman P W 1967 *Phys. Rev.* **155** 796

[72] Cristensen D V, Trier F, Chen Y Z, Smith A, Nygård J and Pryds N 2013 *Appl. Phys. Lett.* **102** 021602